Performance Improvement of DSS-13 34-Meter Beam-Waveguide Antenna Using the JPL Microwave Holography Methodology

D. J. Rochblatt and B. L. Seidel
Ground Antennas and Facilities Engineering Section

This article describes the application of the microwave holography technique to DSS 13. A companion article in this issue (Rochblatt) provides a detailed explanation of the methodology. The project goal of obtaining a rigging-angle surface rms error of 0.43 mm or better was met. The JPL-developed holography algorithms enabled a reduction of the surface error of the DSS-13 antenna from the optically set 0.83-mm axial rms error down to 0.40-mm rms, providing an additional 4.1 dB of performance at 32 GHz.

I. Introduction

The microwave holography technique, when applied to reflector antennas, provides a methodology for examining several critical parameters of the antenna under test [1,2]. The holographically derived information is then used to improve the antenna's RF performance. At DSS 13, more than 4 dB of improvement was obtained at 32 GHz by adjusting the surface of the antenna based on the holographic measurements. Data to aid in the understanding of gravity loading, bypass structural impact, and panel manufacturing contour were obtained. The goal of obtaining a rigging angle surface rms of 0.43 mm or better was achieved. Microwave holography has been demonstrated to be a required tool for initiating, and likely for maintaining, an operational DSN Ka-band (32-GHz) ground antenna capability [3]. Microwave holography has now been applied to all of the 34-m high efficiency (HEF) and 70-m antennas in the Deep Space Network. The raw data (the observable) for this technique constitute the complex far-field pattern of the antenna under test.

The DSS-13 holography plan called for measurements to be first made at the Cassegrain (f1) focus of the antenna to optimize the subreflector position (Fig. 1), evaluate the antenna main reflector, and, if necessary, reset the surface. Following the f1 measurements, the RF test package [4] was to be moved to the beam-waveguide (f3) focus of the antenna (Fig. 2). The f3 measurements, when differenced from the f1 measurements, would provide insight into the performance of the beam waveguide. Measurements made at several elevation angles would aid in the study of structural deformation due to gravitational effects.

This article describes the measurements made at the f1 focus using a data acquisition system loaned to JPL by the

contractor, Eikontech, Ltd. of England. These data were then transferred to the JPL HP-1000/A900 computer and reduced using JPL-developed (Rochblatt) algorithms. The data analysis software was developed in the Antenna and Microwave Development Group of the Ground Antennas and Facilities Engineering Section [1]. A contractual difficulty precluded making holography measurements at f3.

The information obtained from the JPL analysis algorithms was successfully applied. The subreflector position was verified and the rms surface error of the optically set DSS-13 antenna was substantially reduced. The holographically set surface is better than the specified project goal set forth in the *Functional Requirements Document*[1]. The improved antenna surface was verified by both additional holographic and X-band (8.45-GHz) and Ka-band (32-GHz) efficiency measurements. The adjusted surface provides an estimated 4.1-dB improvement in performance at Ka-band (32 GHz), relative to the as-found (optically set) surface. It is estimated that an additional performance improvement of 0.6 dB is possible at 32 GHz over all elevation angles by replacing the panels in rings 8 and 9 with the correctly shaped panels (see the Appendix). It is concluded that holography played a vital and time-efficient role in obtaining a 34-m antenna with an aperture efficiency of 52 percent at Ka-band.

II. Holographic Measurements and Results

In August and September 1990, a total of 24 holography measurements were attempted from the f1 focus of the new DSS-13 beam-waveguide (BWG) antenna. Strong continuous wave (CW) signals obtained from geostationary satellites were used as far-field sources [3,5]. Three different geostationary satellites were successfully scanned, producing four successful high- and medium-resolution data sets at elevation angles of 46.5 deg, 37 deg, and 12.7 deg. The measurements obtained indeed provided the necessary subreflector position information and panel setting information. The measurements also provided a look at the adjusted surface of the antenna, information regarding the exact shape of panels, and information about the gravity performance of the structure at a low elevation angle that revealed the effect of the bypass BWG shroud interaction with the structure. The holographic antenna measurements used satellite signal and ephemeris information supplied by several commercial companies: GTE-operated GSTAR W103, GE-operated SatComm K1, and ComSat-operated Intelsat V.

[1] R. Sniffin and G. Wood, *DSS-13 Functional Requirements Document*, JPL D-8449 (internal document), Jet Propulsion Laboratory, Pasadena, California, May 13, 1989.

The inability of the initially implemented servo system to provide precision pointing at the level of the winds experienced during the observations (24 to 48 km/hr, 15 to 30 mph) resulted in the failure of most of the scans. The results of the four successful high- and medium-resolution scans are reported here. Scan JPL106 was a high-resolution scan that provided the first high-resolution look at the surface of the optically set antenna, as well as provided subreflector position error. This scan was used for deriving the required panel setting information and for predicting the best achievable surface rms error. Scan JPL110 was also a high-resolution scan and provided the after-adjustment look at the surface of the antenna. Scans JPL113 and JPL123 provided surface maps of the antenna at two additional elevation angles (37 deg and 12.7 deg, respectively). The last scan, JPL123 at 12.7-deg elevation, provided valuable information for the structural modeling specialists. These four scans are summarized in Table 1.

It is known that the indicated rms error of the antenna surface is affected by the weakly illuminated outer portion of the dish. When the outer edge of the antenna is included in the analysis, the calculated surface rms error is larger than that obtained from analysis of the strongly illuminated portion of the dish. Functionally, the outer 0.6 m of the antenna radius is a noise shield. The rms error obtained from analysis of the central 32 meters of the antenna is therefore more representative of the actual surface than the rms obtained from examination of the full 34-m dish. The rms values for both the full and the central 32 meters of the antenna are included in Table 1. It is estimated that the 1σ error of the rms (central 32 m) is approximately ± 0.05 mm.

The holographic measurement program at DSS 13 started with measurements taken at an elevation angle of about 46.5 deg. High-resolution scan JPL106 supplied the data required for verifying the subreflector position, analyzing the antenna surface, and providing the panel setting information. The surface images, derived from the aperture plane phase, represent the antenna surface deviations from the ideal in the surface normal direction. In the images, the subreflector, the tripod and its shadows, and the bypass beam waveguide are intentionally masked out. The remaining surface is overlaid with an outline of each reflecting panel. The surface error information is shown in pseudocolor with red and blue indicating the high and low deviations, respectively. Figure 3 shows the surface error map of the central 32 meters of the DSS-13 antenna surface as found on August 28, 1990, by scan JPL106. The main reflector surface normal rms error was found to be 0.88 mm (0.77-mm axial) at a resolution of 0.32 m.

The indicated rms increases as the lateral resolution of the measurement increases. This is an expected result, as there is less area averaging occurring as the resolution increases. The asymptotic or infinite-resolution rms can be estimated by analyzing the scan data at varying resolutions.

Slobin[2] has estimated that the rms error derived by holography high-resolution (0.32-m) scans is 8 percent lower than the infinite resolution rms. That estimate will be used here for consistency. [Since scan JPL123 (12.7-deg elevation) was taken at medium (0.80 m) resolution, a 19-percent correction is applied to this scan.[3]]

After accounting for blockage, the holography data analysis software computes both the normal and the axial rms surface errors. Note that the ratio of the axial to normal rms error depends on the precise distribution of the errors. Therefore, the ratio and, hence, the effective slope are somewhat different for each scan. The holography-based analysis computes an effective average slope for the DSS-13 antenna surface of approximately 30 deg. For high-resolution scans, the infinite resolution axial (1/2 path length) rms error can then be approximated by the relationship

$$\text{axial rms error} = \text{normal rms error} \times 1.08\cos(30\ \text{deg})$$

The above provides a good rule-of-thumb working relationship between the measured high-resolution (0.32-m) normal and the infinite-resolution axial rms surface errors.

Figure 4 shows the predicted surface error map, representing the best achievable surface that would have resulted if the 1716 screws were adjusted precisely as specified by the software. The surface normal rms of this predicted antenna is 0.36 mm at a resolution of 0.32 m. The image reveals that panels in rings 8 and 9 are deformed. A detailed analysis showed that the deformations detected in rings 8 and 9 are due to the fact that the panels used on DSS 13 are of the DSS-15 design shape[4] (see the Appendix for more details). The decision to use DSS-15 panel molds on DSS 13 was made early during the project for budget reasons. Note that the present software moves panels as rigid bodies and that further improvement is possible by properly shaping the individual panels.

The panel setting information derived from scan JPL-106 was applied to the surface panel adjusting screws. As a scheduling expedient it was decided to adjust the surface panels by turning the adjusting screws to the nearest 1/8 of a turn (0.16 mm).[5] Screws requiring adjustment of less than $\pm 1/8$ of a turn were not touched.

The surface error map shown in Fig. 5 was measured on September 7, 1990, after panel resetting (scan JPL110). The deformed panels in rings 8 and 9, as well as many of the other predicted features, are clearly confirmed. The rms surface error achieved by holography-based panel adjustment is 0.45-mm surface normal (0.39-mm axial) at a resolution of 0.32 m. This is equivalent to an infinite-resolution axial rms error of 0.42 mm. This rms error not only exceeds the specification, it also exceeds the goal set forth in the *Functional Requirements Document.* A higher than normal noise level in scan JPL110 leads one to believe that the achieved rms surface error is actually somewhat lower than indicated by this measurement. Indeed, scan JPL113 (Fig. 6), taken at a 37-deg elevation angle, reveals a surface-normal rms error of 0.43 mm and an axial error of 0.37 mm, giving an infinite-resolution axial error of 0.40 mm. Efficiency measurements indicate the 45-deg rigging angle surface to be better than the 37-deg elevation angle surface. One can therefore conclude that, at the rigging angle, the holographically set antenna surface actually has an infinite-resolution axial rms error of slightly less than 0.40 mm.

As shown in Fig. 7, the posthholography surface provides a performance improvement of about 0.2 dB at 8.45 GHz, increasing to 4.1 dB at 32 GHz. The DSS-13 surface specifications, along with the corresponding efficiency calculations and measurements, are summarized in Table 2.

Tables 3 through 6 contain X-band and Ka-band calculations of antenna efficiency. The results are obtained by applying Ruze to the holographically obtained axial rms surface error[6,7] values along with other known block-

[2] S. Slobin, private communication, Jet Propulsion Laboratory, Pasadena, California.

[3] D. J. Rochblatt, *Predicted Performance for DSS-13 at 12.7 Degrees Elevation with Bypass Removal,* JPL IOM 3328-0110 (internal document), Jet Propulsion Laboratory, Pasadena, California, August 28, 1991.

[4] S. Stewart, D. J. Rochblatt, and B. L. Seidel, *The Effect of Using DSS-15 Main Reflector Panels on the DSS-13 BWG Antenna,* JPL IOM 3328-91-0147 (internal document), Jet Propulsion Laboratory, Pasadena, California, November 8, 1991.

[5] B. L. Seidel and D. J. Rochblatt, *DSS-13 BWG Antenna Project, Phase I Final Report, Chapter 4: Microwave Holography,* JPL D-8451 (internal document), Jet Propulsion Laboratory, Pasadena, California, May 15, 1991.

[6] The axial rms surface errors are equal to the 1/2 path-length errors in the familiar form of the Ruze gain-degradation factor $k_g = \exp -[4\pi\epsilon/\delta]^2$. In this expression, ϵ is the 1/2 path error and δ is the wavelength.

[7] Stewart, Rochblatt, and Seidel, op. cit.

ages and losses. These calculated efficiencies are compared to the radiometrically obtained measurements of efficiency. The surface error map shown in Fig. 8 was derived from medium-resolution (0.80-m) holography measurements made on September 18, 1990, at an elevation angle of 12.7 deg (scan JPL123). The surface-normal rms error at this low elevation angle and resolution is 0.50 mm. The corresponding axial- and infinite-resolution axial rms errors are 0.43 mm and an estimated 0.55 mm, respectively. The holography measurements indicate that the subreflector is displaced from the optimum position by 5 mm laterally and 0.4 mm axially at the 12.7-deg elevation angle (see Table 1). A physical optics computation reveals 0.25 dB of performance loss at 32 GHz for this amount of subreflector displacement. Adding this 0.25 dB of performance loss to the measured 39.4-percent antenna efficiency results in a computed performance of 41.7 percent at this elevation angle.

III. Future Work

The holographically set antenna surface already exceeds the specification set forth in the *Functional Requirements Document*. However, fine-tuning the main reflector surface would yield at least another 0.25 dB of improved Ka-band (32-GHz) performance. Careful subreflector positioning might provide another 0.25 dB of performance at low elevation angles. When developed and applied, panel unbending techniques would further improve aperture efficiency.

By examining the holography data, it was found that using DSS-15 panel molds for manufacturing DSS-13 panels caused an additional 0.6-dB performance loss over all elevation angles [7]. Thus, even better results could be obtained in the future given another pass of holography adjustments along with some panel unbending.

It is also necessary to return to DSS 13 to make the f3 measurements that were not obtained in Phase 1. Information obtained from these measurements, when differenced from those obtained at f1, would provide an important holographic diagnosis of the BWG effects on the antenna system.

Finally, a microwave holography measurement system will be provided for aligning and maintaining all of the DSN tracking antennas [8]. Such a system is indispensable to an operational Ka-band ground antenna capability in support of future deep space missions and, in fact, is needed even for an X-band network. Microwave holography is a station-time and cost-effective means for providing this support.

IV. Conclusion

The principal f1 holography goal of obtaining a rigging angle surface rms error of 0.5 mm or better at DSS 13 has been met. The JPL-developed holography algorithms, the RF test package, and the concept (and execution) of f1 holography measurements on a BWG antenna worked extremely well. JPL microwave holography enabled reducing the surface error of the DSS-13 antenna from the optically set as-found 0.83-mm axial rms error down to a very respectable 0.40-mm rms. This holographically improved surface not only exceeds the *Functional Requirements Document* specification (0.61 mm), it also exceeds the 0.43-mm goal. The holographically set antenna surface provides an additional 4.1 dB of performance at 32 GHz.

Acknowledgments

The authors thank Dan Bathker for his many helpful technical discussions and contributions. In addition, thanks are due to Manuel Franco from JPL and Paul Wright and Eric Schoessow from Eikontech, Ltd. for helping with the holographic measurements at DSS 13.

References

[1] D. J. Rochblatt, "A Methodology for Diagnostics and Performance Improvement for Large Reflector Antennas Using Microwave Holography," *Proceedings of the Antenna Measurement Technique Association*, AMTA, Boulder, Colorado, pp. 1-7–1-12, October 7, 1991.

[2] D. J. Rochblatt, "A Microwave Holography Methodology for Diagnostics and Performance Improvement for Large Reflector Antennas," *TDA Progress Report 42-108*, vol. October–December 1991, Jet Propulsion Laboratory, Pasadena, California, pp. 235–252, February 15, 1992.

[3] D. J. Rochblatt, "System Analysis for DSN Microwave Antenna Holography," *TDA Progress Report 42-97*, vol. January–March 1989, Jet Propulsion Laboratory, Pasadena, California, pp. 132–157, May 15, 1989.

[4] T. Y. Otoshi, S. R. Stewart, and M. M. Franco, "A Portable Ku-band Front-End Test Package for Beam-Waveguide Antenna Performance Evaluation," *TDA Progress Report 42-107*, vol. July–September 1991, Jet Propulsion Laboratory, Pasadena, California, pp. 73–80, November 15, 1991.

[5] D. J. Rochblatt and Y. Rahmat-Samii, "Effects of Measurement Errors on Microwave Antenna Holography," *IEEE Transactions on Antennas and Propagation*, vol. 39, no. 7, pp. 933–942, July 1991.

[6] D. J. Rochblatt, Y. Rahmat-Samii, and J. H. Mumford, "DSN Microwave Antenna Holography Part II: Data Processing and Display of High Resolution Effective Maps," *TDA Progress Report 42-87*, vol. July–September 1986, Jet Propulsion Laboratory, Pasadena, California, pp. 92–97, November 15, 1986.

[7] D. J. Rochblatt and B. L. Seidel, "DSN Microwave Antenna Holography," *TDA Progress Report 42-76*, vol. October–December 1983, Jet Propulsion Laboratory, Pasadena, California, pp. 27–42, February 15, 1984.

[8] D. J. Rochblatt, "System Requirements for NASA Deep Space Network Microwave Antenna Holography," paper presented at the International Symposium on Antenna and Propagation, Tokyo, Japan, August 22–25, 1989.

Table 1. Results of DSS-13 microwave holography at f1.

	Scan JPL106	Scan JPL110	Scan JPL113	Scan JPL123
Satellite	GSTAR W103	GSTAR W103	SatComm K1	Intelsat V
Elevation angle	46.5	46.5	37.0	12.7
Measurement frequency, GHz	12.198	12.198	12.198	11.701
Surface	Mechanical	Mechanical	Mechanical	Eff[a]
Array size	127 x 127	127 x 127	127 x 127	51 x 51
Resolution, m	0.32	0.32	0.32	0.80
RMS, mm				
Surface normal				
Full antenna	1.07	0.58	0.71	0.66
Central 32 m	0.88	0.45	0.43	0.50
Axial				
Central 32 m	0.77	0.39	0.37	0.43
Infinite resolution	0.83	0.42	0.40	0.55
Estimated surface error				
Loss, dB				
Ruze				
2.30 GHz	0.028	0.007	0.006	0.012
8.34 GHz	0.375	0.096	0.087	0.160
32.00 GHz	5.375	1.376	1.248	2.360
Estimated subreflector				
Position error, mm				
X	−0.53	+0.28	+1.07	−1.88
Y	−1.06	−1.41	−3.07	−4.72
Z	+1.10	+1.13	+0.66	+0.39

[a] Eff: Effective surface error map without removal of the feed/subreflector phase function [6].

Table 2. DSS-13 rigging angle surface specifications, efficiency calculations and measurements at f1.

Antenna surface	RMS, mm	Calculated/Measured aperture efficiency, percent	
		8.45 GHz	32.0 GHz
As found	0.83	71.7/71.9	21.6/[a]
Specified	0.61	74.6/[a]	38.3/[a]
Goal	0.43	76.4/[a]	53.6/[a]
After reset	0.40	76.6/75.4	56.0/52.3
Potential (existing panels)	0.36	76.9/[a]	59.2/[a]
Potential (replacing panels in rings 8 and 9)	0.28	77.4/[a]	65.4/[a]

Notes:

(1) Efficiency estimates include 0.07-dB I^2R loss at 8.45 GHz and 0.27-dB I^2R loss at 32 GHz.

(2) Both the 8.45-GHz and the 32-GHz efficiency estimates include 186.6 m^2 of aperture blockage.

(3) The measured efficiency values (supplied by Slobin) are derived from radiometric measurements.

(4) Given a perfect main reflector surface, the estimated X- and Ka-band efficiencies would be 78.2 percent and 74.7 percent, respectively. This difference is due to the different I^2R losses at the two frequencies.

[a] N/A or no measured data available.

Table 3. Comparison of holography-based efficiency estimate with measured value: X-band postadjustment at rigging angle (using the 37-deg infinite resolution rms value).

DSS-13 34-m BWG antenna, 8.45-GHz at 46-deg elevation			
Gross area			907.9 m^2
Less			
Noise shield	64.7 m^2		
S/R blockage	9.0 m^2		
Strut blockage	74.4 m^2		
Bypass blockage	23.5 m^2		
Illumination taper	15.0 m^2		
Subtotal		186.6 m^2	
Ruze loss, 0.40 mm		14.3 m^2	
S/R position loss		Negligible	
Subtotal effective area			707.0 m^2
I^2R loss, X-band, 0.07 dB		11.3 m^2	
Net effective area			695.7 m^2
Area efficiency			
Estimated			76.6 percent
Measured			75.4 percent

Table 4. Comparison of holography-based efficiency estimate with measured value: X-band postadjustment at 12.7 deg.

DSS-13 34-m BWG antenna, 8.45-GHz at 12.7-deg elevation			
Gross area			907.9 m^2
Less			
Noise shield	64.7 m^2		
S/R blockage	9.0 m^2		
Strut blockage	74.4 m^2		
Bypass blockage	23.5 m^2		
Illumination taper	15.0 m^2		
Subtotal		186.6 m^2	
Ruze loss, 0.40 mm		26.8 m^2	
S/R position loss		Negligible	
Subtotal effective area			694.5 m^2
I^2R loss, X-band, 0.07 dB		11.2 m^2	
Net effective area			683.3 m^2
Area efficiency			
Estimated			75.3 percent
Measured			74.0 percent

Table 5. Comparison of holography-based efficiency estimate with measured value: Ka-band postadjustment at rigging angle (using the 37-deg infinite resolution rms value).

DSS-13 34-m BWG antenna, 32-GHz at rigging angle			
Gross area			907.9 m^2
Less			
Noise shield	64.7 m^2		
S/R blockage	9.0 m^2		
Strut blockage	74.4 m^2		
Bypass blockage	23.5 m^2		
Illumination taper	15.0 m^2		
Subtotal		186.6 m^2	
Ruze loss, 0.40 mm		180.2 m^2	
S/R position loss		Negligible	
Subtotal effective area			541.1 m^2
I^2R loss, X-band, 0.27 dB		32.6 m^2	
Net effective area			508.5 m^2
Area efficiency			
Estimated			56.0 percent
Measured			52.3 percent

Table 6. Comparison of holography-based efficiency estimate with measured value: Ka-band postadjustment at 12.7 deg.

DSS-13 34-m BWG antenna, 32-GHz at 12.7-deg elevation			
Gross area			907.9 m^2
Less			
Noise shield	64.7 m^2		
S/R blockage	9.0 m^2		
Strut blockage	74.4 m^2		
Bypass blockage	23.5 m^2		
Illumination taper	15.0 m^2		
Subtotal		186.6 m^2	
Ruze loss, 0.55 mm		302.4 m^2	
S/R position loss, 0.25 dB		25.7 m^2	
Subtotal effective area			393.2 m^2
I^2R loss, X-band, 0.27 dB		26.2 m^2	
Net effective area			367 m^2
Area efficiency			
Estimated			40.4 percent
Measured			39.4 percent

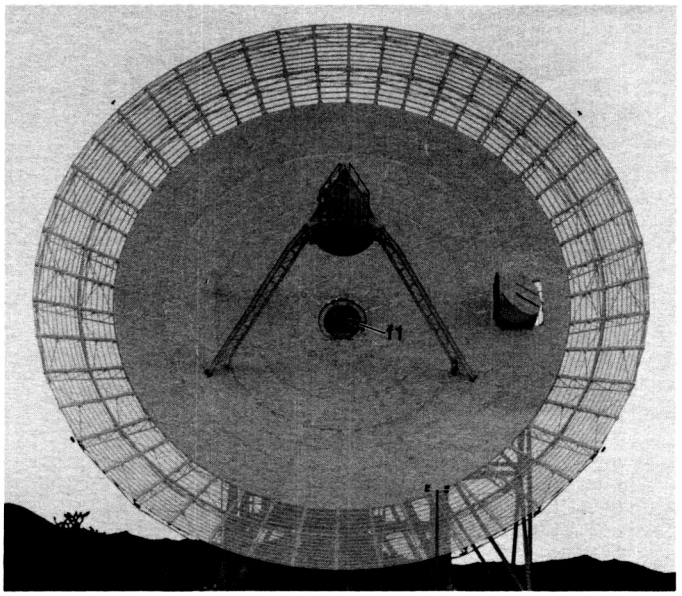

Fig. 1. DSS-13 34-m BWG antenna showing the Ku-band horn feed at the f1 position at the Cassegrain focus.

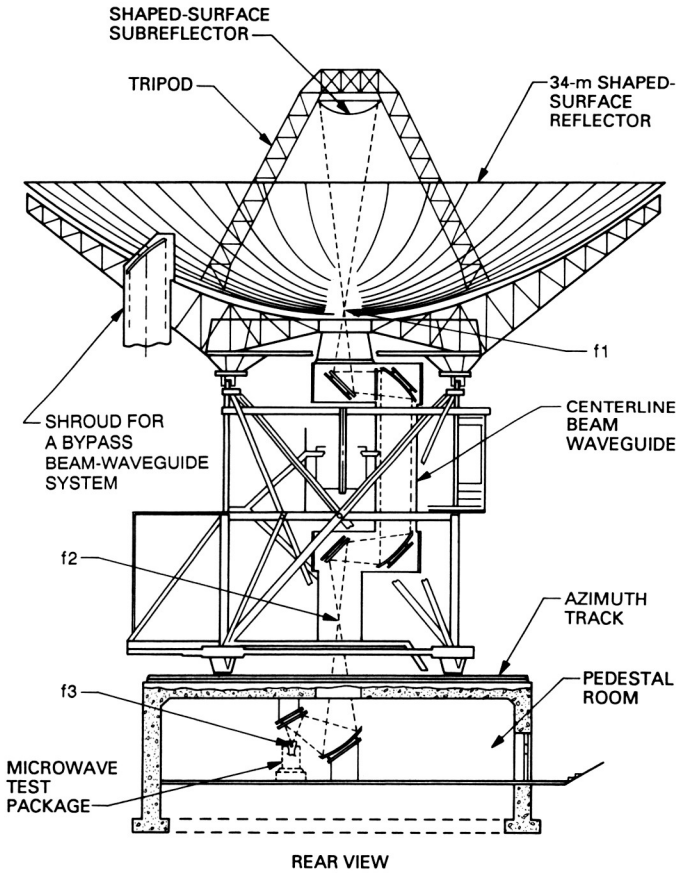

Fig. 2. DSS-13 antenna showing f3 beam waveguide focus.

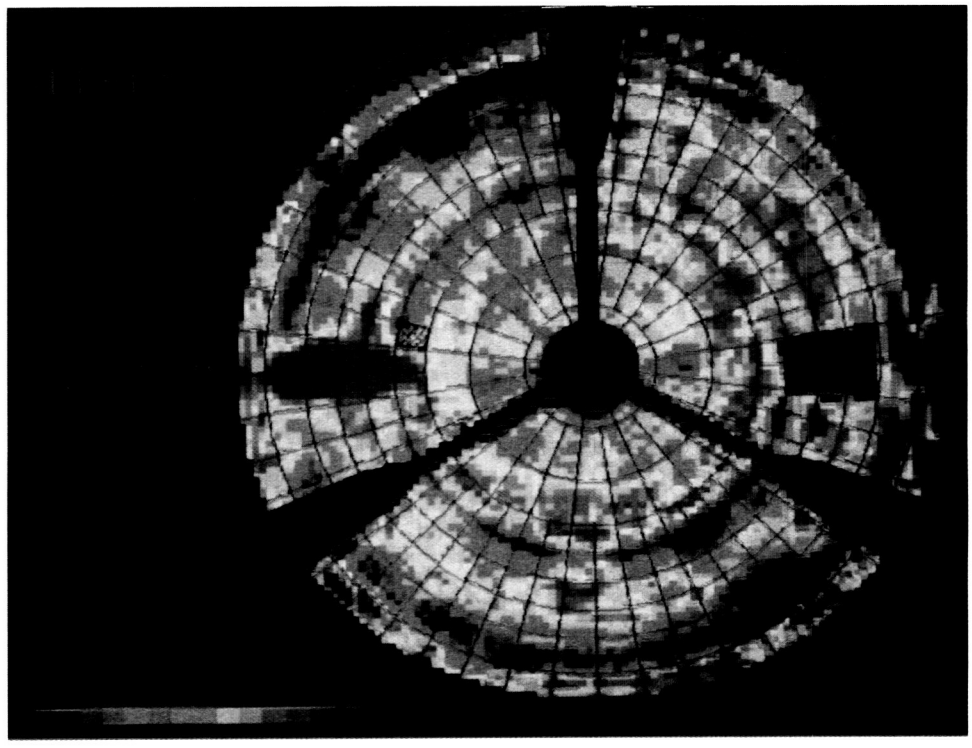

Fig. 3. High-resolution (0.32-m) error map of the central 32 m of the DSS-13 antenna surface at 46-deg elevation, before panel setting, as derived from scan JPL106 (August 28, 1990).

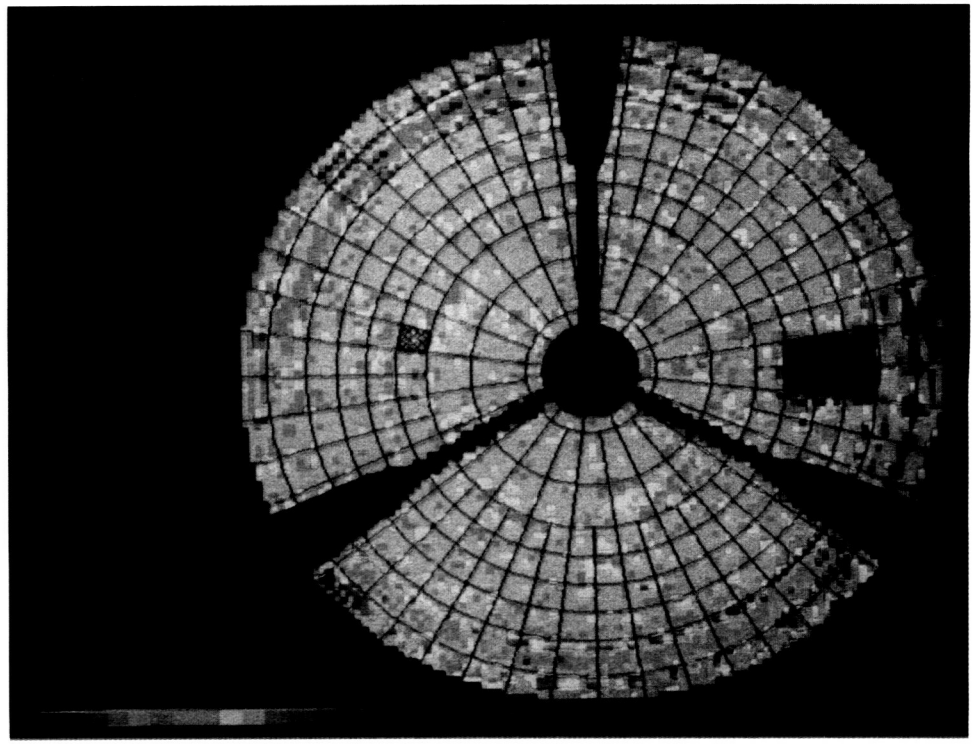

Fig. 4. Predicted surface error map derived from scan JPL106. This represents the best achievable rigging angle surface that would have resulted if the 1716 screws were adjusted precisely as specified by the software.

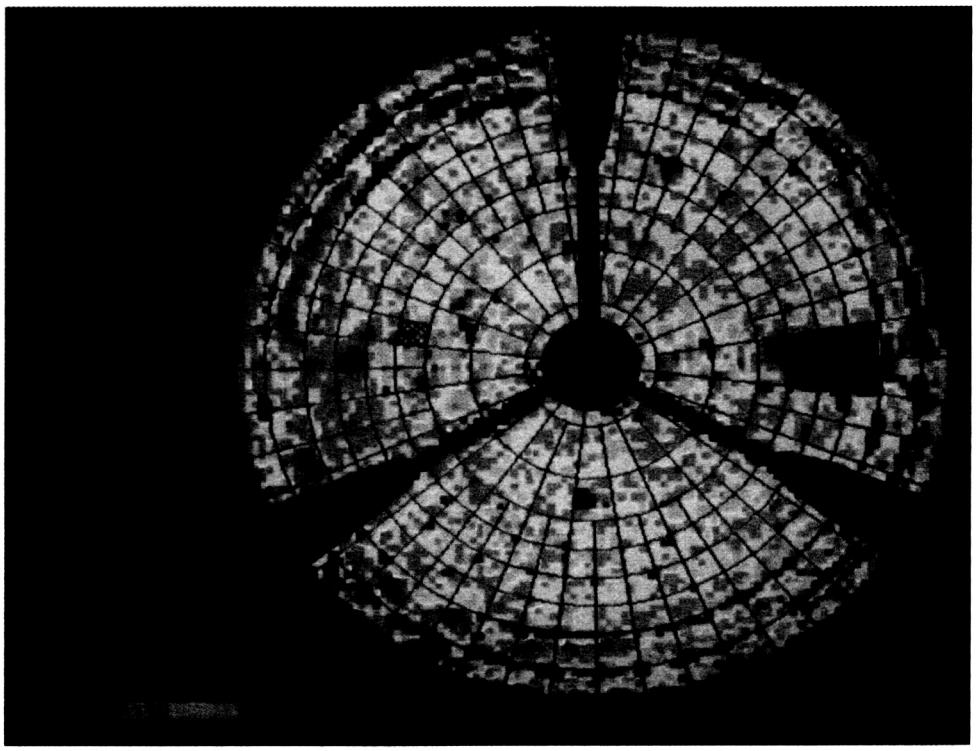

Fig. 5. High-resolution (0.32-m) error map of the central 32 m of the DSS-13 antenna surface at 46-deg elevation, after panel setting, as derived from scan JPL110 (September 7, 1990).

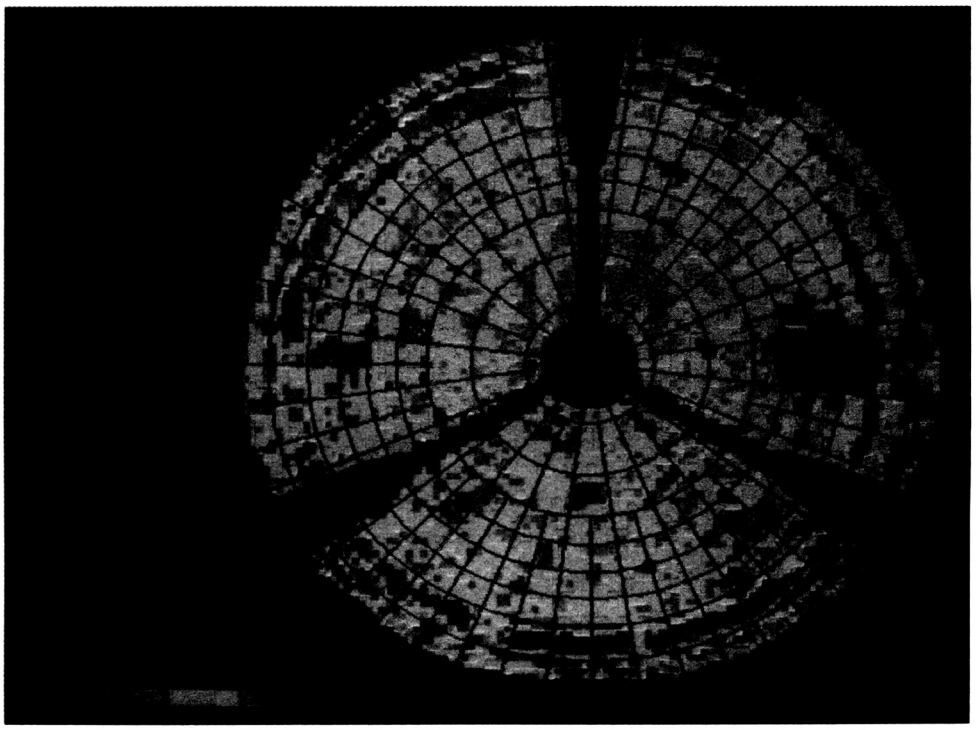

Fig. 6. High-resolution (0.32-m) error map of the central 32 m of the DSS-13 antenna surface at 37-deg elevation, after panel setting, as derived from scan JPL113 (September 11, 1990).

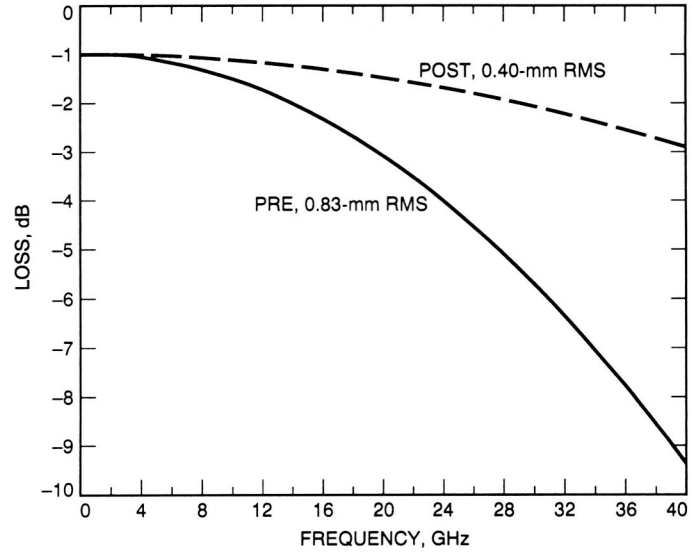

Fig. 7. Loss due to surface error versus frequency. The loss indicated in these curves is based on aperture blockage and surface roughness. No attempt was made to include I^2R losses. An estimated improvement in antenna performance of approximately 4.1 dB was achieved at 32 GHz after panel resetting.

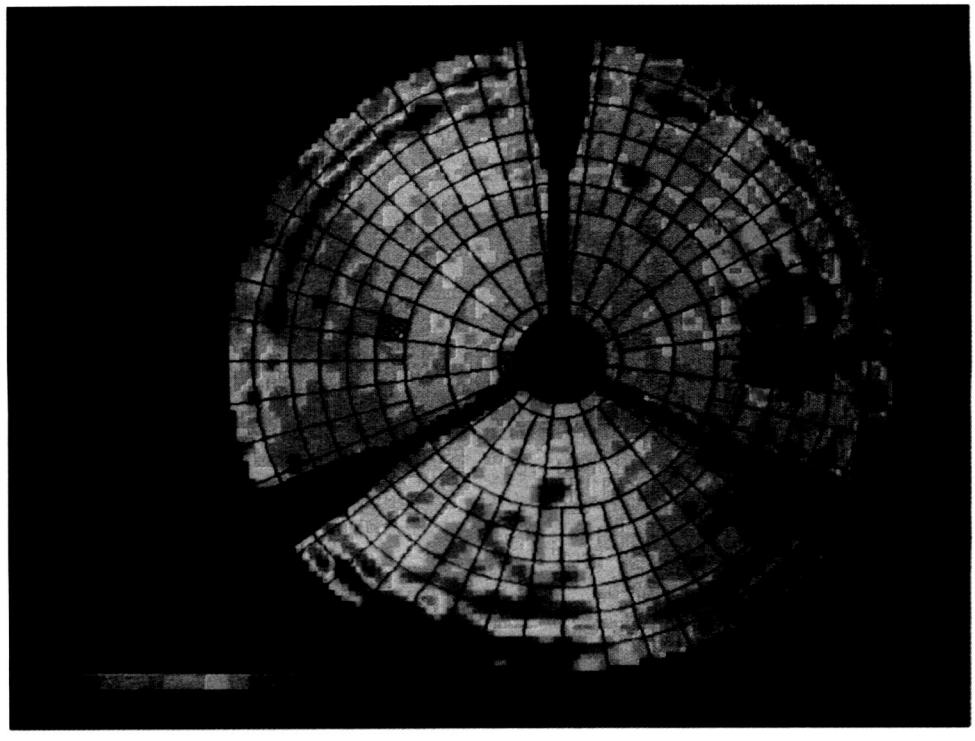

Fig. 8. Medium (0.80-m) resolution error map of the central 32 m of the DSS-13 antenna surface at 12.7-deg elevation, after panel setting, as derived from scan JPL123 (September 18, 1990).

Appendix

The Effect of Using DSS-15 Main Reflector Panel Molds for Fabrication of DSS-13 Panels

S. Stewart, D. J. Rochblatt, and B. L. Seidel

In 1988, when the new DSS-13 BWG antenna project was still in the planning stages, it was decided that the main reflector panels for the DSS-13 antenna should be made from the available molds that were used to make the main reflector panels for the DSS-15 antenna. The differences in the shape of the panels were thought to be minor, and it was believed they would not significantly affect the required (per the *Functional Requirements Document*) performance of the new research and development antenna.

Looking at each of the nine panel rings individually and assuming that the panels on the DSS-13 antenna were made accurately from the DSS-15 manufacturing contours, the panels were mathematically best-fitted to the DSS-13 design contour. The axial errors between these two contours were calculated for each of the nine panel rings by subtracting the reference DSS-13 required shape from the DSS-15 panel contour.

The errors in the first seven panel rings are minor and cause no significant performance loss at 32 GHz. The errors in panels 8 and 9 (Figs. A-1 and A-2, respectively) are much more sizable and contribute noticeably to RF performance degradation at 32 GHz. (It should be noted that the outer half of panel 9 is a noise shield and should not be viewed as contributing to the RF gain performance.)

The next step was to look at the holography data measured at the f1 focal point in order to determine if these mechanical errors of as much as 0.79 mm were detected. Several holography data sets were examined, comprising measurements made both prior to and after panel resetting, as well as computed prediction models. Figure A-3 shows the mechanical surface error map that was obtained from the holographic measurements made on the DSS-13 antenna on August 28, 1990, prior to panel resetting. This map describes the surface errors of the as-found optically set antenna. The magnitude of the various mechanical surface errors across the dish make detection of the errors due only to the misshaped panels impossible from this map. The predicted best achievable antenna surface was derived from this mechanical surface error map by the holography software and is shown in Fig. A-4. The software makes no attempt to untwist distorted panels, but rather adjusts them, in a least-squares fit, as rigid bodies. The result of the fitting represents the best rms antenna surface achievable without unbending panels. The remaining surface errors are due primarily to the shape of the panels.

Figures A-5 and A-6 present the inner seven rings and the outer two rings of the predicted surface, respectively. The deformed panels in rings 8 and 9 are clearly noticeable and account for the large rms surface error of 0.60 mm for that part of the dish compared to the much lower rms surface error of 0.24 mm for the inner seven rings. It should be noted that 0.24 mm is the rms of the inner seven rings of the best or predicted surface, and can only be obtained when the panel-screw-adjustment computer listings are followed exactly. In actuality, 0.28-mm rms was achieved for this portion of the dish surface. It is interesting to note that the rss difference of the actual (0.28 mm) and the best achievable surfaces (0.24 mm) is approximately equal to the screw adjusting accuracy, hence, 1/8 of a turn (0.16 mm versus 0.14 mm).

Figures A-7 and A-8 are plots for rings 8 and 9, respectively, of the constructed average symmetric phase error function from the predicted surface error map and the analytically derived feed phase function at the measurement frequency of 12.198 GHz. The figures clearly indicate that the signature of the feed phase function, which is frequency dependent, is properly absent in the constructed function derived from the predicted surface error map. Therefore, the confidence is high that the feed phase function has been accurately accounted for. Figures A-9 and A-10 show the holographically derived surface errors for rings 8 and 9, respectively, overlaid on the predicted mechanical surface errors for these panels. These plots show good agreement between the manufacturing contour and the holography measurements.

The current antenna surface has an rms error of 0.28 mm for the inner seven panel rings, 0.60 mm for rings 8 and 9 together, and 0.40 mm for all of the antenna, excluding the noise shield.

The errors in the DSS-13 BWG antenna surface in the outer two panel rings have been measured accurately and are noticeable in 32-GHz performance. Estimates have

been made as to the possible gain improvement that would be obtained if these panels were replaced by panels that had surface errors on the order of those seen on the inner seven panel rings. The outer two rings incorporate 37 percent of the aperture area, not including the noise shield. If this area of the antenna were to have its rms error decreased from 0.60 mm to 0.28 mm, the increase in antenna gain would be 0.6 dB at 32 GHz. The present Ka-band area efficiency of 52 percent at f1 would increase to 60 percent if the 0.6-dB opportunity is pursued.

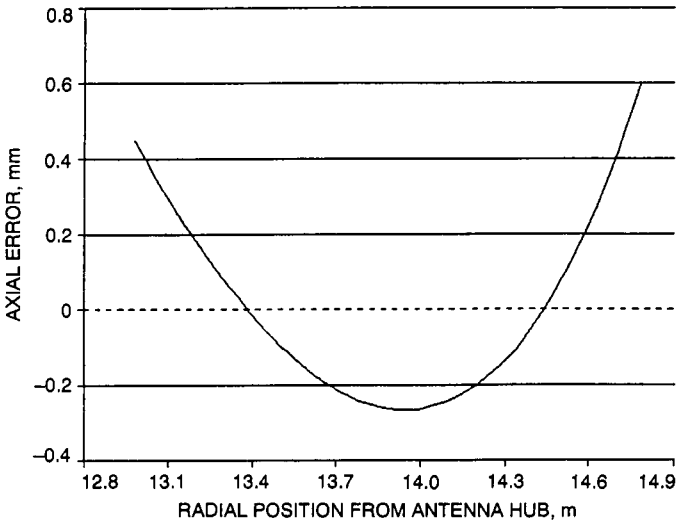

Fig. A-1. Mechanical error in DSS-13 main reflector surface panel 8.

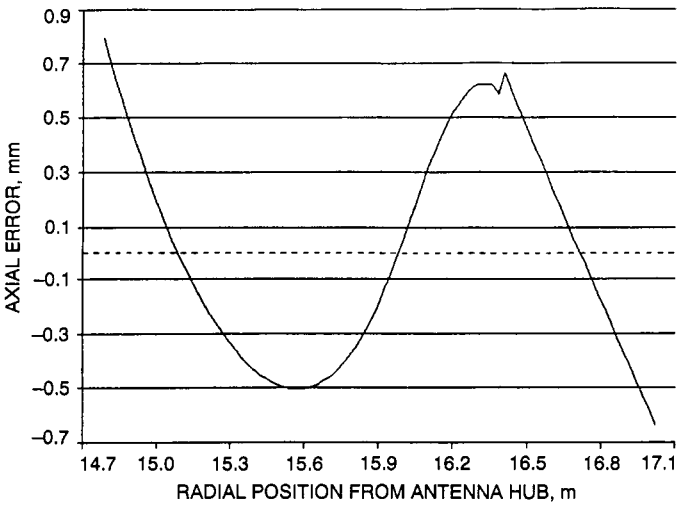

Fig. A-2. Mechanical error in DSS-13 main reflector surface panel 9.

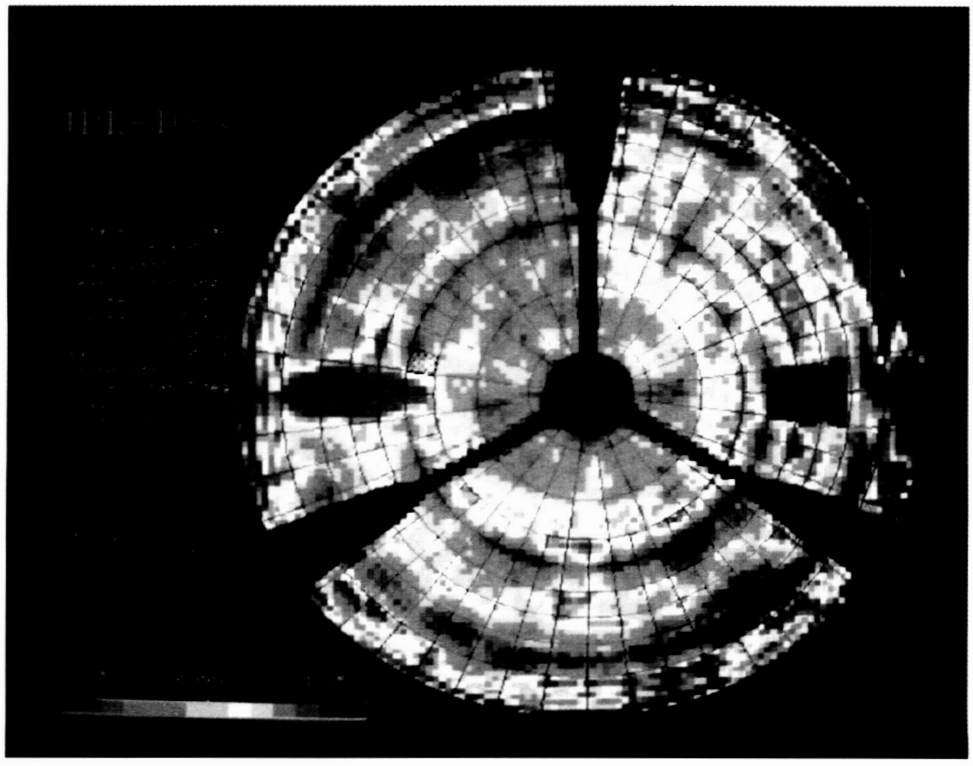

Fig. A-3. High-resolution mechanical error map of DSS-13 antenna surface at 46.5-deg elevation before panel setting.

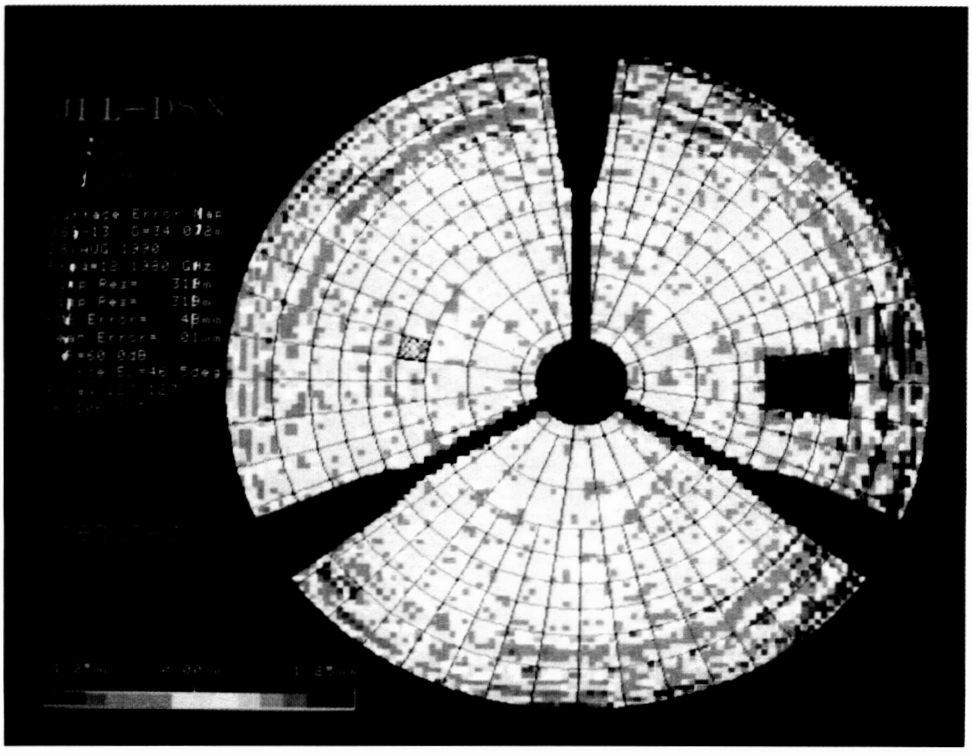

Fig. A-4. Predicted surface error map representing the best achievable rigging angle surface resulting from precision adjustment of set screws.

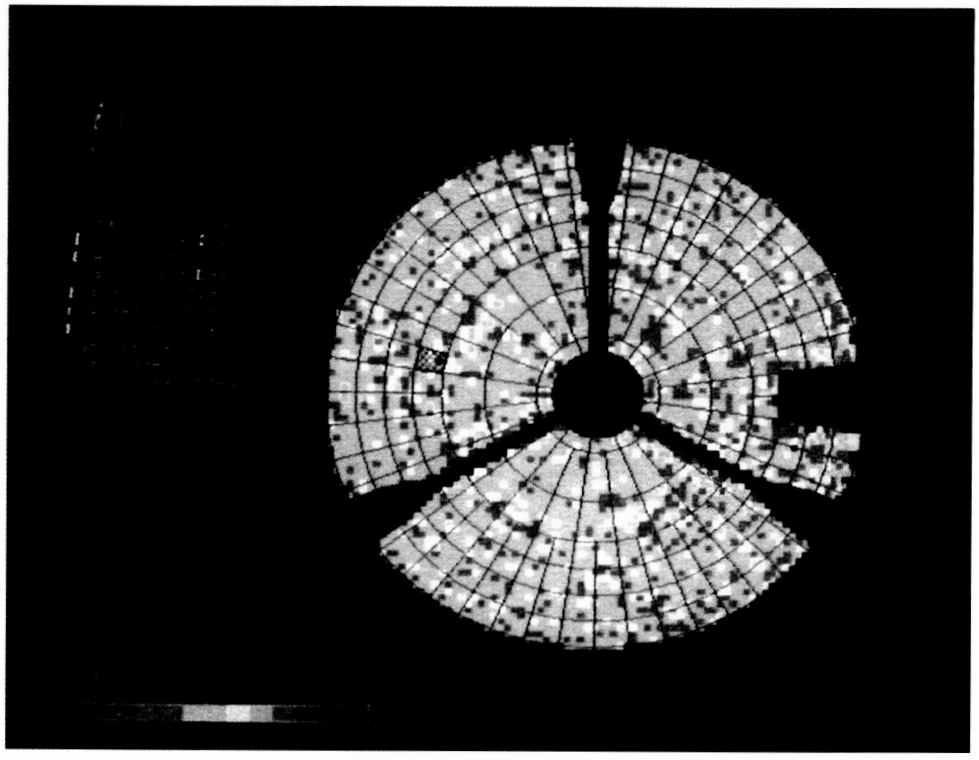

Fig. A-5. Inner seven panel rings with infinite resolution axial rms error of 0.24 mm.

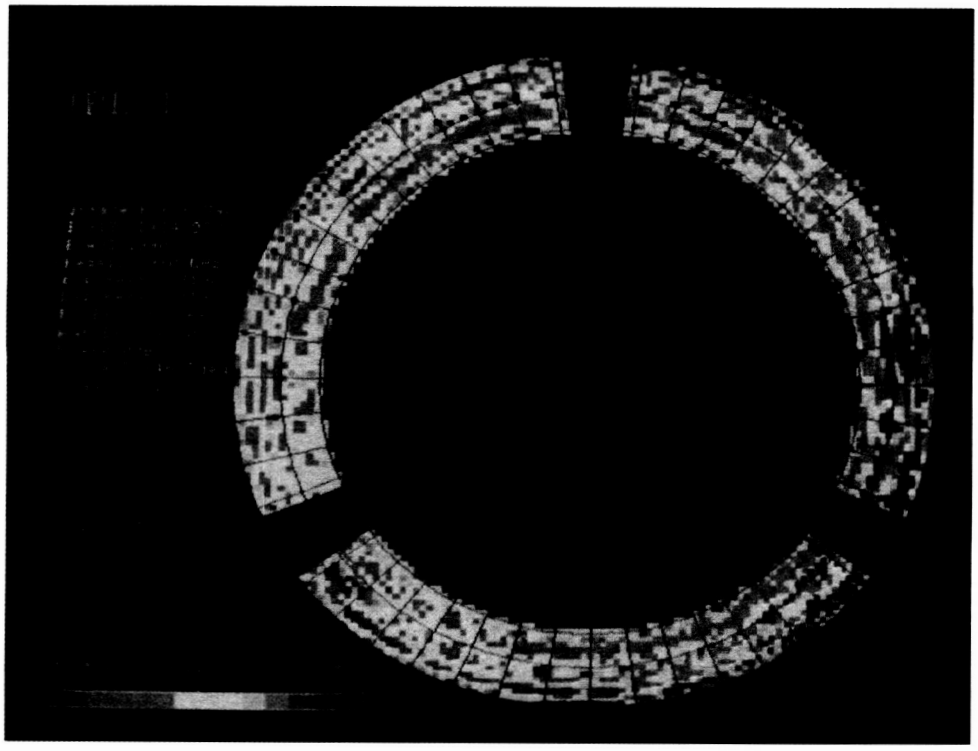

Fig. A-6. Panel rings 8 and 9 with infinite resolution axial rms error of 0.60 mm.

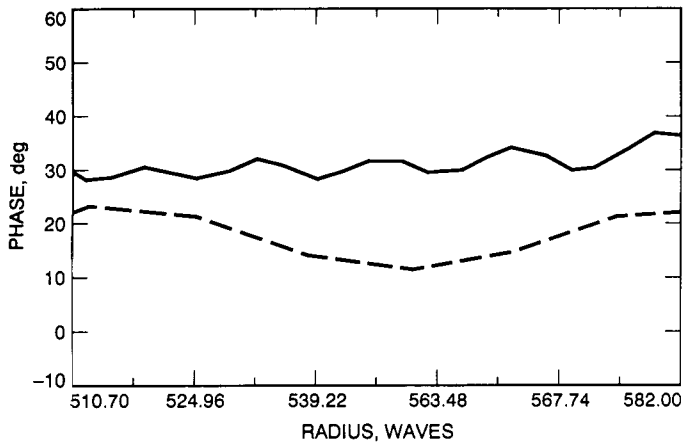

Fig. A-7. Panel ring 8—feed phase function (solid line) and constructed phase function (dashed line).

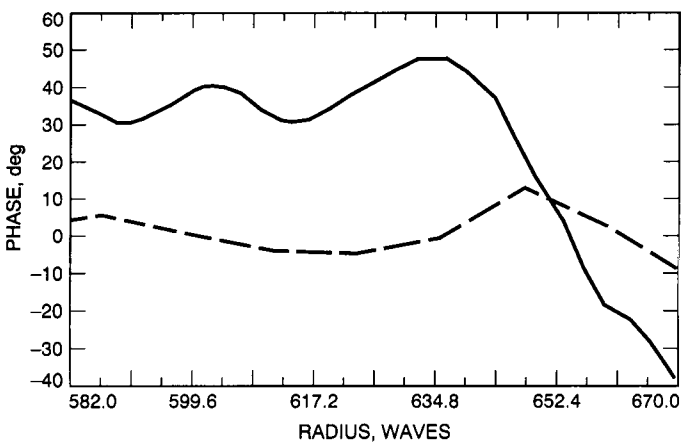

Fig. A-8. Panel ring 9—feed phase function (solid line) and constructed phase function (dashed line).

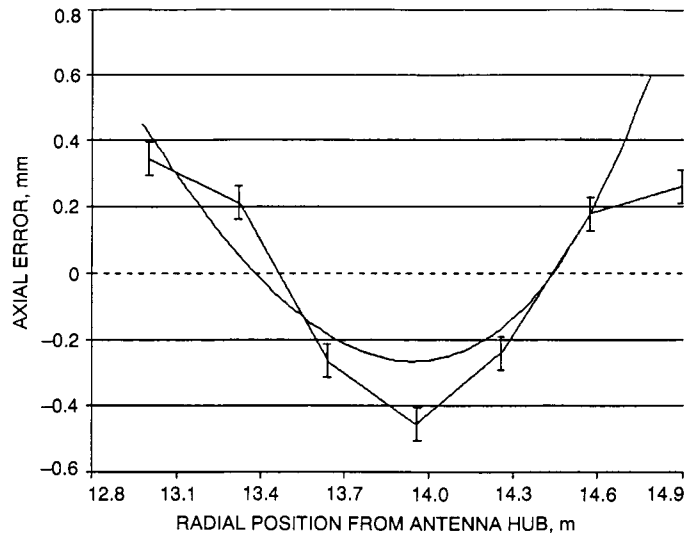

Fig. A-9. Mechanical error in panel ring 8 with holographically derived average phase error function.

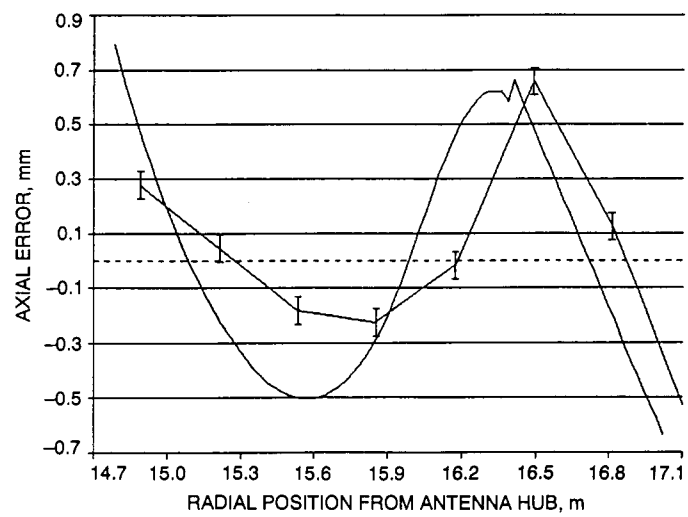

Fig. A-10. Mechanical error in panel ring 9 with holographically derived average phase error function.